

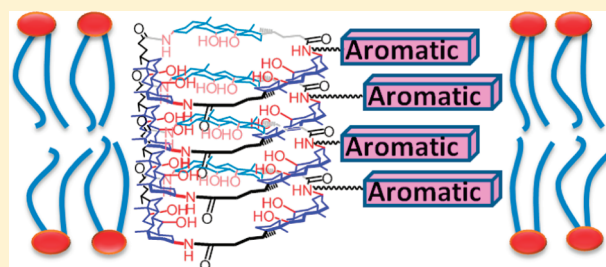
Aromatically Functionalized Cyclic Tricholate Macrocycles: Aggregation, Transmembrane Pore Formation, Flexibility, and Cooperativity

Lakmini Widanapathirana and Yan Zhao*

Department of Chemistry, Iowa State University, Ames, Iowa 50011-3111, United States

Supporting Information

ABSTRACT: The aggregation of macrocyclic oligocholates with introverted hydrophilic groups and aromatic side chains was studied by fluorescence spectroscopy and liposome leakage assays. Comparison between the solution and the membrane phase afforded insight into the solvophobic driven aggregation. The macrocycles stacked over one another in lipid membranes to form transmembrane nanopores, driven by a strong tendency of the water molecules in the interior of the amphiphilic macrocycles to aggregate in a nonpolar environment. The aromatic side chains provided spectroscopic signatures for stacking, as well as additional driving force for the aggregation. Smaller, more rigid macrocycles stacked better than larger, more flexible ones because the cholate building blocks in the latter could rotate outward and diminish the conformation needed for the water-templated hydrophobic stacking. The acceptor–acceptor interactions among naphthalenediimide (NDI) groups were more effective than the pyrene–NDI donor–acceptor interactions in promoting the transmembrane pore formation of the oligocholate macrocycles.



evidence for the pore formation includes strong cooperativity among four macrocycles in the transport activity, ineffectiveness of the linear trimer, a counterintuitive increase of glucose transport with increasing hydrophobicity of the membrane, an unusual faster transport of maltotriose over glucose, shutting down of the pore-transport mechanism with guests whose cross-section was larger than the pore diameter, and excimer formation in pyrene-labeled macrocycles.

INTRODUCTION

Chemists have long been intrigued by the abilities of biological transporters to move molecules from one side of the membrane to the other by channels or pores.¹ The process is important to not only many key biofunctions but also a number of practical applications including drug delivery,¹ sensing,² and catalysis.³ In recent years, synthetic transmembrane pores with an inner diameter of 1 nm or larger have attracted the attention of many researchers.⁴ The research is expected to improve our understanding of the biological pore-forming mechanisms, as well as providing useful materials for practical applications.

Unlike ion channels frequently prepared from flexible structures such as crown ethers,⁵ pore-forming materials need to have significant rigidity to withstand the external membrane pressure to keep the internal pore from collapsing.⁶ A number of successful synthetic nanopores have been constructed following this principle. Ghadiri, for example, utilized hydrogen-bonding interactions to assemble cyclic D/L-peptides into nanopores large enough for glucose and glutamic acid to pass through.⁷ Matile and co-workers developed an extremely versatile class of β -barrel pores from oligo(phenylene) derivatives^{3,8} and demonstrated their applications in artificial photosynthesis⁹ and catalysis.³ Other reported examples include the porphyrin-based nanopores by Satake and Kobuke,¹⁰ the π -stacked aromatic heterocycles by Gong,¹¹ Fyles's metal-coordinated nanopores,¹² and the guanosine quartet-based giant ion channels by Davis.¹³

We recently reported that amphiphilic macrocyclic oligocholates such as **1** could form transmembrane nanopores.¹⁴ Key

The pore formation was proposed to be promoted by hydrophobic interactions, which typically work in aqueous instead of hydrocarbon-based media. Macrocycle **1** has an internal hydrophilic cavity nearly 1 nm across. Being overall hydrophobic, compound **1** prefers a membrane over an aqueous environment. Once the molecule enters the membrane, however, the amphiphilic macrocycle needs to solvate its introverted hydrophilic groups by water instead of the lipid hydrocarbon. The conflicting solvation requirements of the introverted hydrophilic groups and the exterior hydrocarbon framework are solved when multiple macrocycles stack over one another to form a transmembrane pore (Figure 1). The arrangement allows the water molecules inside the macrocycles to interact with one another, solvate the polar groups of the cholates, and still exchange readily with the bulk water. The driving force for the stacking is essentially the associative interactions among the "activated" water molecules in the interior of the macrocycles located in a highly

Received: March 6, 2012
Published: April 23, 2012

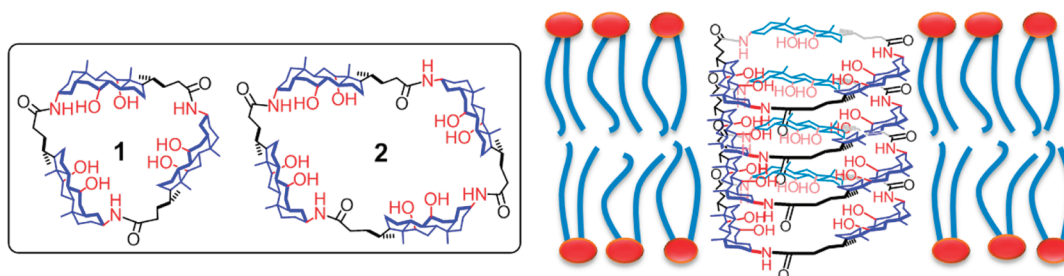
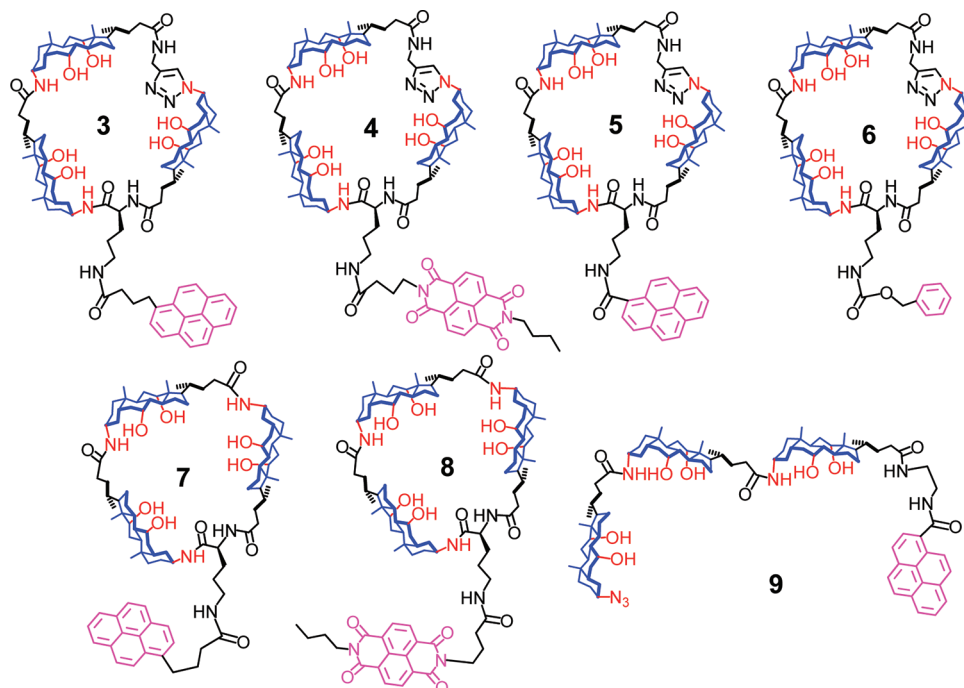


Figure 1. Schematic representation the idealized pore formation of oligocholate macrocycle 1 in a lipid bilayer membrane.

Chart 1. Aromatically Functionalized Oligocholate Macrocycle (2–8) Used in the Current Study



hydrophobic environment. The exchange of the water molecules inside the pore with those in the bulk outside the membrane may also be important, as the entropic cost for trapping a single water molecule can be as high as 2 kcal/mol under certain conditions.¹⁵

Aromatic interactions are among the most important tools in supramolecular chemistry.¹⁶ The interactions enabled the construction of many interesting materials including foldamers^{16,17} and have already been utilized in synthetic pore-forming materials.^{3,8–13} The interactions have a number of components including electrostatic, van der Waals, and solvophobic interactions. Depending on the electronic nature of the aromatic systems and the media involved, the interacting partners may adopt edge-to-face, offset stacked, or face-to-face stacked configurations.¹⁶

In this paper, we report several oligocholate macrocycles with aromatic side chains.¹⁸ A main objective of the research was to design aromatically functionalized oligocholate pore-forming materials in which the aromatic interactions and the above-mentioned hydrophobic interactions could work cooperatively. The oligocholate macrocycles were inspired by our linear oligocholate foldamers whose folding is driven by solvophobic interactions in mixed organic solvents.¹⁹ In fact, the folding of the oligocholate foldamers and the stacking of the cholate macrocycles are driven by essentially the same solvophobic

interactions.^{14a} Although it is clear that organic solvents and lipid bilayers are very different media, it is often not clear *how* different environments impact the outcome and especially the mechanism of molecular recognition. When it comes to investigation of molecular recognition in difficult-to-study environments such as lipid membranes, researchers frequently extrapolate learning from solution studies to the new environment. For these reasons, we are particularly interested in the effects of environments on the intermolecular interactions of the macrocycles. The study revealed a number of important factors in the pore-forming mechanism including the rigidity of the macrocycle, the lipid composition, and the type of π systems most effective in promoting the hydrophobic stacking of the oligocholate macrocycles.

RESULTS AND DISCUSSION

Design and Syntheses of Oligocholate Macrocycles.

Chart 1 shows the aromatically functionalized oligocholates synthesized in this study. Compound 3 was previously prepared as a fluorescently labeled macrocycle to study the stacking mechanism by fluorescence spectroscopy.^{14a} Macrocycle 4 carries a naphthalenediimide (NDI) group instead of pyrene on the side chain. The NDI group is an electron-deficient π system, known to interact strongly with π donors.^{16,17} Its ability to quench the pyrene fluorescence allows us to study its

Scheme 1. Syntheses of Macrocycles 7 and 8

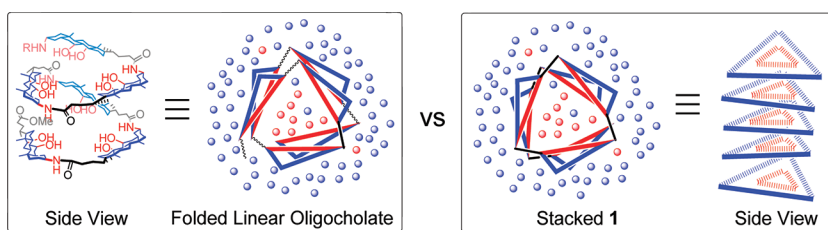
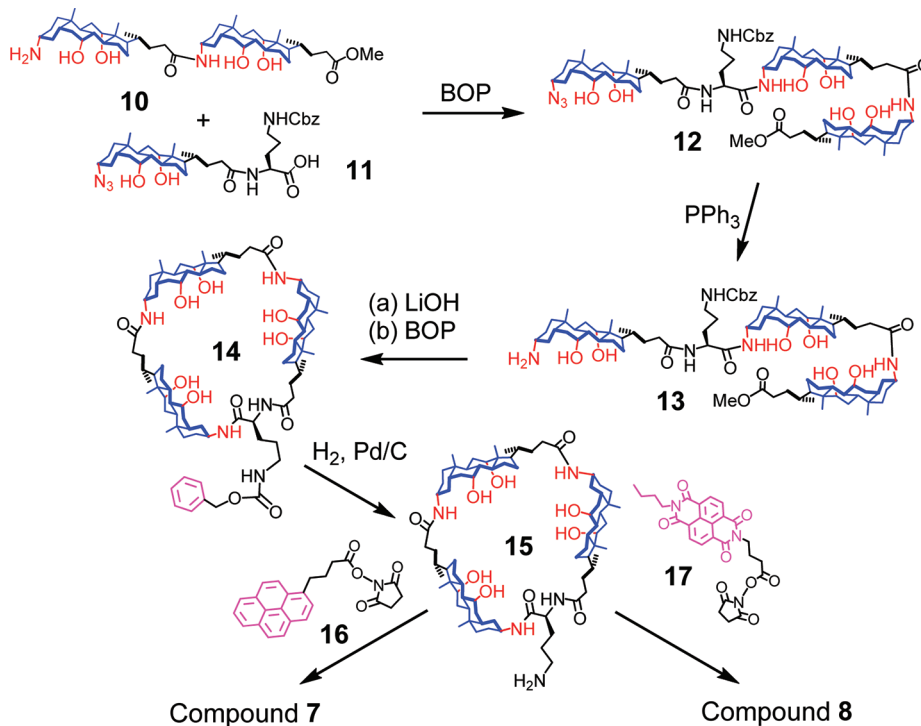


Figure 2. Schematic representation of the solvophobic driven folding of a linear oligocholate and aggregation of macrocyclic oligocholate 1. The red and blue circles represent polar and nonpolar solvent molecules, respectively. (Reprinted with permission from ref 25. Copyright 2011. American Chemical Society, Washington, DC).

interaction with pyrene-labeled macrocycles such as 3 and 5 by fluorescence spectroscopy.

Both 3 and 5 have the pyrenyl group on the side chain; their difference is in the number of atoms in between the oligocholate macrocycle and the aromatic group. Whereas 3 and 4 are matched nearly perfectly regarding the length of the tether in between the macrocycle and the aromatic side chain, 5 and 4 are mismatched. If the cholate macrocycles stack up to engage in the aforementioned hydrophobic interactions, the aromatic side chains would have difficulty achieving the face-to-face configuration for the aromatic donor–acceptor interactions.¹⁶ The molecules thus were designed to test whether the electron-donor–acceptor interactions would work cooperatively with the hydrophobic, water-templated stacking of the oligocholate macrocycles.

Compounds 3–5 were all synthesized from the previously reported 6,^{14a} which has a Cbz-protected L-ornithine. All of the macrocycles were cyclized by the highly efficient alkyne–azide click reaction.²⁰ The cyclization was employed partly because the synthesis of linear, amide-linked oligocholates always leaves behind an azide and an ester at the chain ends.²¹ The most efficient way to synthesize an oligocholate macrocycle, therefore, is to hydrolyze the ester, couple it to an alkyne-

terminated amine such as propargyl amine, and cyclize through the click reaction.

Another way of macrocyclization is to couple an amine–carboxyl-terminated linear oligocholate by amide coupling. Scheme 1 shows the syntheses of macrocycles 7 and 8 using this method. First, the amine-terminated dimer 10 and a cholate monomer with a Cbz-protected L-ornithine (11) were coupled to afford linear trimer 12 using benzotriazol-1-ylxytris(dimethylamino)phosphonium hexafluorophosphate (BOP) as the coupling reagent. The azido group of 12 was reduced by triphenylphosphine to afford amine–ester terminated 13, which was hydrolyzed into the carboxylate and cyclized using BOP. After deprotection of the Cbz group, the amine derivative 15 was allowed to react with activated esters 16 and 17 to afford the all-amide-linked oligocholate macrocycles 7 and 8, respectively.

Aggregation of Oligocholate Macrocycles in Solution.

The oligocholate macrocycles were inspired by our linear oligocholate foldamers. Both the folding of linear oligocholates and the aggregation of the oligocholate macrocycles are driven by the same form of solvophobic interactions.^{14a} In a nonpolar solvent containing a few percent of a polar solvent, the extended conformer of a linear oligocholate is disfavored

because of its exposed polar faces to the nonpolar solvent, the major component of the solvent mixture. By folding into a helix with introverted hydrophilic groups, the oligocholate creates a hydrophilic internal cavity filled disproportionately with the polar solvent (Figure 2, left panel). The arrangement satisfies the needs of the cholate polar groups to be solvated by polar instead of nonpolar solvent. Meanwhile, the nonpolar surface of the oligocholate is exposed to the nonpolar solvent and some polar solvent molecules are able to reside in a hydrophilic microenvironment. Since the folded oligocholate prefers a trimeric periodicity,^{18a,21} macrocycle **1** essentially is a cross-section of the folded helix. The solvophobic forces that drive the folding of the linear oligocholate will promote the stacking of the macrocycles in the *z*-direction (Figure 2, right panel).

The most “folding-friendly” solvents for the oligocholate foldamers are ternary mixtures such as 2:1 hexane/ethyl acetate with a small amount of methanol.^{19a} Hexane is immiscible with methanol but miscible with ethyl acetate. A large amount of hexane in the mixture thus makes it easy to phase-separate methanol from the bulk and reduces the energetic cost associated with the folding. As the amount of methanol increases, the folded oligocholate typically unfolds, due to the better solvation of the polar groups by the bulk solvent.¹⁹ When the hydrophilic and hydrophobic faces of the linear oligocholates become both well-solvated, the unfolded conformation is more favorable because of its higher conformational entropy.

To understand the stacking of the aromatically functionalized macrocycles, we first performed fluorescence quenching of the pyrene-labeled oligocholates by the NDI-functionalized ones in 2:1 hexane/ethyl acetate with varying percentage of methanol. A small amount of methanol was needed to dissolve the compounds in nonpolar solvents. As described earlier, the polar solvent also serves to “template” the aggregation of the macrocycles by interacting with one another through hydrogen bonds. Essentially, by interacting with one another and with the polar groups on the internal wall of the stacked nanopore via hydrogen bonds, the methanol molecules within the pore act as a solvophobic “glue” to pull the amphiphilic macrocycles together.

Figure 3a shows the normalized emission intensity of pyrene-labeled oligocholates (i.e., **3**, **5**, and **9**) in the presence of 1 equiv of NDI-functionalized **4** in the ternary solvents. The emission intensity was normalized to that in 0.5% methanol for all three pairs, allowing us to compare the different

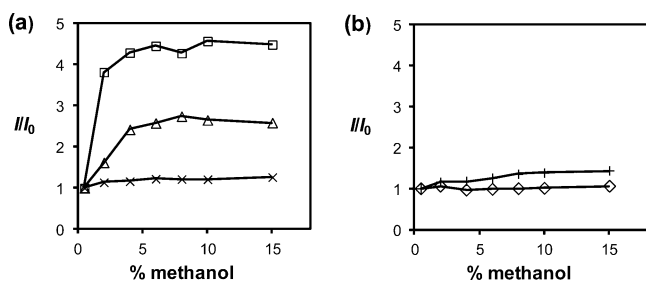


Figure 3. (a) Normalized emission intensity at 397 nm of a 1:1 mixture of **3** and **4** (□), **5** and **4** (△), and **9** and **4** (×) in 2:1 hexane/ethyl acetate with different percentages of methanol. (b) Normalized emission intensity of a 1:1 mixture of **7** and **8** (◇) and **9** and **8** (+) in 2:1 hexane/ethyl acetate with different percentages of methanol. The emission intensity in 0.5% methanol was taken as the I_0 . $\lambda_{\text{ex}} = 350$ nm. [Oligocholate] = 2.0 μM .

fluorophores more accurately.²² The solvophobic driving force is expected to be the strongest in 0.5% methanol. An increase of methanol lowers the driving force for the aggregation and should reduce the quenching of pyrene by NDI and enhances the pyrene emission.

Indeed, both the matched pair (**3** and **4**, □) and the mismatched pair (**5** and **4**, △) displayed stronger emission in higher methanol solvents. Thus, aggregation-induced quenching did exist in low methanol solvents. As a control experiment, we studied the quenching of the linear tricholate **9** by the NDI-labeled **4**. Because linear oligocholates can only fold cooperatively with at least five cholate units,²¹ trimer **9** cannot adopt the reverse micelle-like conformation with introverted hydrophilic groups. Stacking should thus be very difficult, if not impossible, with the 1:1 mixture of **9** and **4**. Consistent with our stacking model, the control pair (×) showed nearly constant pyrene emission over the same solvent change, indicating that the cyclic motif was necessary for the quenching in low methanol solvents and that the change of pyrene emission in the first two mixtures was *not* caused by a generic solvent effect.

Figure 3b shows the same quenching study done with the all-amide-linked macrocycles (**7** and **8**). Likewise, we performed the control experiment with the linear tricholate **9**. In our hands, both pairs displayed small or negligible changes in fluorescence intensity during the methanol titration. The results were quite surprising to us, as we thought that rigidity of the macrocycles was beneficial to the solvent-induced aggregation.^{14a} (We will come back to this point toward the end of the paper.)

Aggregation of Oligocholate Macrocycles in Lipid Membranes. We could not perform solvent titration in membranes as in organic solutions. Instead, we varied the concentration of the oligocholates in the membrane. As demonstrated by our previous study, the oligocholate macrocycles aggregate in membranes only above a critical aggregation concentration (CAC).^{14a} Quenching of the pyrene emission should thus become significant above the CAC for the pyrene–NDI mixed pairs.

Figure 4a shows the emission intensity of the 1:1 mixture of **3/4** (□) and **5/4** (△) in 1,2-dilauroyl-*sn*-glycero-3-phosphocholine (DLPC) membranes. The intensity was normalized to that of the same mixture at 10 mol % concentration in the membrane. The 10 mol % concentration is well above the CACs of **1** or **2**^{14a} and should correspond to the fully aggregated form. As expected, both mixtures displayed much higher emission intensity at lower concentrations, suggesting that strong quenching did exist at higher concentrations of the oligocholates in the membrane. Most interestingly, the CAC of the matched pair (**3** and **4**, □, ~0.5 mol %) was noticeably lower than the mismatched pair (**5** and **4**, △, ~1.0 mol %), evident from the earlier inflection point in the quenching curves for the former. The result agreed well with the stronger quenching found for the matched pair in Figure 2a and suggests that the hydrophobic stacking of the oligocholate macrocycles and the pyrene–NDI aromatic interactions did seem to work together (see later sections for further discussion).

Figure 4b compares the clicked (**3** and **4**, □) and the all-amide pairs (**7** and **8**, ◇), both matched in the length of the tether between the cholate macrocycle and the aromatic side chain. The concentration-dependent aggregation was evident in both cases as shown by the strong emission at lower concentrations and a sharp decrease at ca. 0.5 mol %

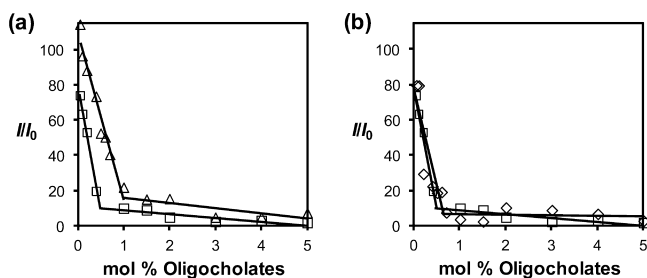


Figure 4. (a) Normalized emission intensity at 398 nm of a 1:1 mixture of 3 and 4 (\square) and 5 and 4 (\triangle) as a function of the molar percentage of the total oligocholates in DLPC membranes. (b) Normalized emission intensity at 398 nm of a 1:1 mixture of 3 and 4 (\square) and 7 and 8 (\diamond) as a function of the molar percent of the total oligocholates in DLPC membranes. The data for 3 and 4 (\square) were shown in both figures for comparison. The emission intensity with $[\text{total oligocholates}]/[\text{phospholipids}] = 1/10$ was taken as the I_0 . $\lambda_{\text{ex}} = 350$ nm. The CACs (in mol % with respect to the phospholipids) were obtained by linear regression of the data points below and above the inflection point in the quenching curves. Because aggregation of two different oligocholate macrocycles involves many different aggregated structures, the CAC is actually the CAC probed by the coassembly of the NDI- and pyrene-labeled macrocycles. $[\text{Oligocholate}] = 2.0 \mu\text{M}$.

concentration of the oligocholates. The experiment, however, was not able to distinguish the two types of macrocycles, as both pairs gave similar CACs.

According to the pore-forming mechanism, the aggregation of the macrocyclic oligocholates should occur more easily in more hydrophobic membranes.^{14a} We, therefore, performed the similar quenching studies in 1-palmitoyl-2-oleoyl-*sn*-glycero-3-phosphocholine (POPC) membranes, which were more hydrophobic than the C12 DLPC membranes.²³ Figure 5 shows the normalized emission intensity of the 1:1 mixture of 3/4, 5/4, and 7/8 in DLPC (blue) and POPC/POPG membranes (red). Assuming that the difference in pyrene emission intensity was not a generic environmental effect—reasonable given the methanol-insensitive emission of pyrene displayed by 9/4 in Figure 3a—the data suggests that significant quenching already existed at low oligocholate concentrations in the POPC

membranes. Aggregation thus was indeed easier in the more hydrophobic membranes.

The hydrophobic aggregational model also predicts that the CACs of the oligocholates should be lower in POPC than in DLPC membranes. The quenching data, nevertheless, did not reveal such a trend. The inflection points of the quenching curves for the POPC membranes in general are difficult to identify (especially in Figure 5c for the all-amide-linked pair). One complication, as mentioned above, might occur because aggregation already took place at low concentrations. We believe another complication comes from the different aggregational propensities of the pyrene and NDI groups in the membranes. As will be shown by the glucose leakage assay, the NDI-labeled macrocycles prefer to self-associate instead of aggregating with the pyrene-functionalized macrocycles in lipid membranes (*vide infra*). Especially in POPC membranes in which the driving force for the aggregation is high, the majority of the NDI-labeled macrocycles (5 and 8) should be involved in self-aggregation instead of interacting with the pyrene-functionalized macrocycles. Fluorescent quenching, consequently, only reports a fraction of the entire aggregational process.

Fortunately, pyrene itself could be used as a probe to monitor the aggregation (although no information can be obtained through this method for the NDI-labeled macrocycles). Because of its long fluorescence lifetime, pyrene can form excimers quite readily even at relative low concentrations.²⁴ Heteroaggregation is no longer an issue when only one type of cyclic oligocholate exists in the membrane. Figure 6 shows the normalized emission spectra of pyrene-labeled macrocycle 7 in three different lipid membranes. In general, the excimer emission at ca. 470 nm increased relative to that of the monomer at 378 nm with higher concentrations of 7 in the membrane. Aggregation of the macrocycle thus was clearly concentration-induced. In the DLPC membrane, the excimer formation was sluggish until the concentration of 7 reached 10 mol % (Figure 6a). In the more hydrophobic POPC/POPG membranes, the excimer formed more easily and the emission at 470 nm increased steadily with an increase in the concentration of the macrocycle. The addition of cholesterol enhanced the pyrene excimer even further. Even at the lowest tested concentration (0.02 mol %), significant excimer formation was observed for compound 7 (Figure 6c).

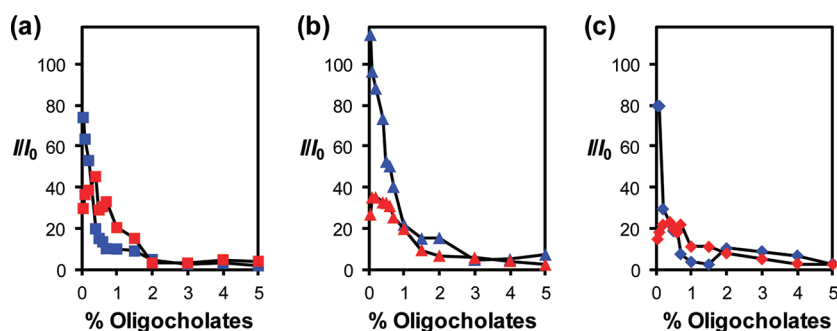


Figure 5. Normalized emission intensity at 398 nm of a 1:1 mixture of (a) 3 and 4, (b) 5 and 4, and (c) 7 and 8 as a function of $[\text{total oligocholates}]/[\text{lipid}]$ ratio in POPC/POPG membranes. The blue and red data points were obtained in DLPC and POPC/POPG membranes, respectively. The emission intensity with $[\text{total oligocholates}]/[\text{phospholipids}] = 1/10$ was taken as the I_0 . $\lambda_{\text{ex}} = 350$ nm. The large unilamellar vesicles (LUVs) were made by detergent dialysis for the DLPC and POPC/POPG membranes with $[\text{total oligocholates}] = 2.0 \mu\text{M}$. The LUVs ($[\text{phospholipids}] = 107 \mu\text{M}$) were made by membrane extrusion with the cholesterol-containing membranes, due to their incompatibility with the detergent dialysis.^{14a}

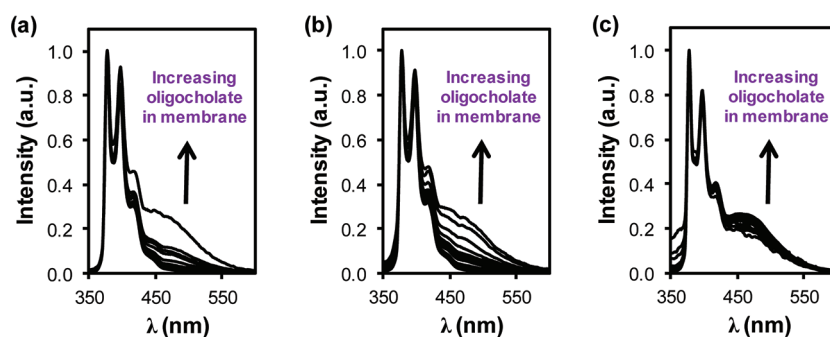


Figure 6. Normalized emission spectrum of **7** in (a) DLPC, (b) POPC/POPG, and (c) POPC/POPG membranes with 30 mol % cholesterol. The molar percentage of **7** in the membrane was from 0.05 to 10% from bottom to top in (a) and (b). The molar percentage of **7** in the membrane was from 0.002 to 10% from bottom to top in (c). $\lambda_{\text{ex}} = 350$ nm. The large unilamellar vesicles (LUVs) were made by detergent dialysis for the DLPC and POPC/POPG membranes with $[\text{oligocholeate}] = 2.0 \mu\text{M}$. The LUVs ($[\text{phospholipids}] = 107 \mu\text{M}$) were made by membrane extrusion with the cholesterol-containing membranes, due to their incompatibility with the detergent dialysis.^{14a}

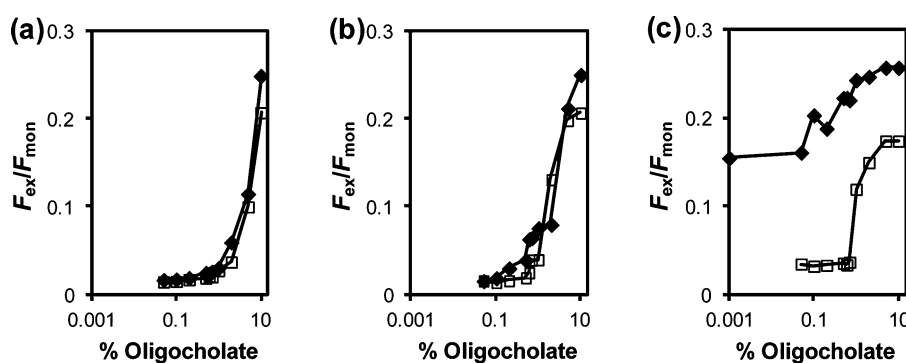


Figure 7. Excimer/monomer ratio (i.e., emission intensity ratio of 470 vs 378 nm) as a function of $[\text{oligocholeate}]/[\text{lipid}]$ ratio in liposomes made of (a) DLPC, (b) POPC/POPG, and (c) POPC/POPG with 30 mol % cholesterol. The data points shown in filled diamonds (◆) and empty squares (□) are for **3** and **7**, respectively. $\lambda_{\text{ex}} = 350$ nm. The liposomes were made by detergent dialysis for the DLPC and POPC/POPG membranes with $[\text{oligocholeate}] = 2.0 \mu\text{M}$. The large unilamellar vesicles (LUVs) were made by detergent dialysis for the DLPC and POPC/POPG membranes with $[\text{oligocholeate}] = 2.0 \mu\text{M}$. The LUVs ($[\text{phospholipids}] = 107 \mu\text{M}$) were made by membrane extrusion with the cholesterol-containing membranes, due to their incompatibility with the detergent dialysis.^{14a}

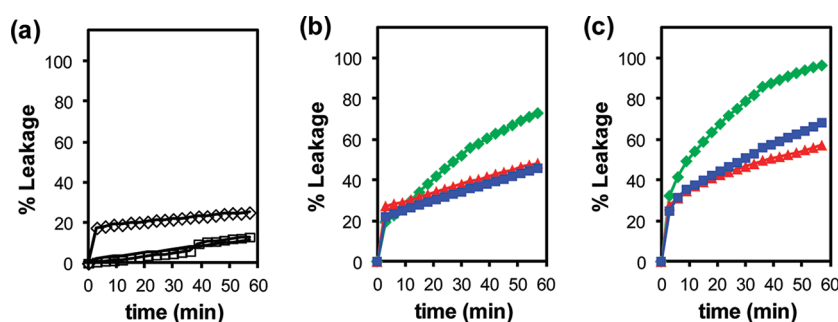


Figure 8. Percent leakage of glucose from (a) POPC/POPG LUVs upon the addition of **3** (Δ), **4** (\diamond), and 1:1 mixture of **3** and **4** (\square), and from (b) POPC/POPG LUVs and (c) POPC/POPG LUVs with 30% cholesterol upon the addition of **7** (red triangle), **8** (green diamond), and 1:1 mixture of **7** and **8** (blue box). $[\text{total oligocholeates}] = 5.0 \mu\text{M}$. $[\text{phospholipids}] = 104 \mu\text{M}$. The liposomes were lysed at 60 min upon addition of 1% Triton X-100.

The excimer formation of the clicked macrocycle **3** was studied previously.^{14a} Figure 7 compares the excimer/monomer ratio of **3** and **7** as a function of the macrocycle concentration in the membrane. In all three cases, the all-amide-linked **7** showed stronger pyrene excimer than the clicked **3**, as indicated by the former's generally higher excimer/monomer ratio at the same concentration. Although the trend was visible in DLPC and POPC/POPG membranes, it was most clear in the most hydrophobic, cholesterol-containing POPC/POPG membranes. The consistently high excimer/monomer ratio in **7**,

even at low concentrations, suggests that the all-amide-linked oligocholeate macrocycle aggregated more easily than the clicked **3** in lipid membranes (Figure 7c).

Glucose Transport by Aromatically Functionalized Oligocholeate Macrocycles. Strong evidence for the stacked nanopores of **1** and **2** was obtained by their transport of sugars across lipid bilayer membranes.^{14a} The internal cavity of **1** is triangularly shaped and ca. 1 nm on the side, large enough for glucose to pass through. In the glucose transport assay, a high concentration (300 mM) of glucose was first trapped inside

large unilamellar vesicles (LUVs).²⁵ After the external glucose was removed by gel filtration, hexokinase, glucose-6-phosphate dehydrogenase, NADP, and ATP were added to liposomal solution. In the absence of transporting agents, the glucose stays inside the LUVs and remains intact. If an added reagent causes leakage of the liposomes, the escaped glucose will be converted by the enzymes to glucose-6-phosphate while NADP will be reduced to NADPH. Because of the fast enzymatic kinetics, the formation of NADPH at 340 nm normally correlates directly with the rate of glucose efflux.^{7a} At the end of the experiments, a nonionic surfactant, Triton X-100, is added to destroy the liposomes and the amount of NADPH formed is used as the reference for 100% leakage.

Figure 8a shows the percent leakage of glucose triggered by the pyrene-labeled clicked macrocycle 3 (Δ), the NDI-labeled 4 (\diamond), and a 1:1 mixture of 3 and 4 (\square). The total concentration of the oligocholates was kept the same (5 μ M) in all of the leakage assays. This concentration was able to cause complete leakage of the glucose with the parent cyclic trimer 1.^{14a} As indicated by the leakage data (Figure 8a), however, all three clicked macrocycles were quite incompetent in comparison to the parent macrocycle, with only the NDI-functionalized 4 showing modest activity.

The all-amide-linked macrocycles had considerably higher activities than the clicked ones (Figure 8b). The glucose leakage at the end of 60 min reached over 70% with the NDI-functionalized 8. The NDI-labeled macrocycle was clearly more potent than either the pyrene-functionalized one or the 1:1 mixture, suggesting that the aromatic interactions of the electron-deficient π system were stronger in the membrane than aromatic donor–acceptor interactions.

An important outcome of the hydrophobically driven pore formation for the oligocholate macrocycles was their counter-intuitive faster transport of glucose in thicker and more hydrophobic membranes.^{14a} Figure 8c shows the leakage profiles caused by the all-amide-linked macrocycles in POPC/POPG membranes with 30 mol % cholesterol. This level of cholesterol is known to increase the hydrophobic thickness of POPC bilayer from 2.58 to 2.99 nm²⁶ and decrease its fluidity.²⁷ Cholesterol-containing bilayers have been shown to be much less permeable to hydrophilic molecules, including glucose.²⁸ Cholesterol incorporation, however, increased the driving force for the hydrophobic stacking interactions of the oligocholate macrocycles and was found to *accelerate* the glucose leakage induced by 1 and 2.^{14a} The effect was once again observed for the amide-linked macrocyclic oligocholates (compare Figures 8b and 8c). In corroboration with the cholesterol-enhanced pyrene excimer-formation (Figure 6c), the leakage data strongly suggest that the same pore-forming mechanism was involved in these experiments.

Environmental Effects on the Intermolecular Interactions of the Oligocholate Macrocycles. The obvious “inconsistency” so far is between the quenching data in solution (Figure 3) and the pyrene excimer/leakage data in lipid membranes (Figures 7 and 8). The former suggests that the clicked macrocycles aggregate more strongly than the all-amide-linked ones in mixed organic solvents, whereas the latter indicates the opposite in lipid membranes.

The solvophobic interactions in the oligocholates derive from the need for the introverted hydrophilic groups to be solvated by polar solvent, as well as the tendency of the polar solvent to avoid contact with the nonpolar environment (Figure 2).^{14a,19} This model predicts that the solvophobic interactions are the

strongest when the polar/nonpolar solvents are least miscible and the polar solvent has a large cohesive energy density (i.e., total intermolecular interactions per unit volume).

The lipid membrane is ideal for the solvophobic driven aggregation.^{14a} Water and the lipid hydrocarbon are completely immiscible, meaning that placing water inside the oligocholate macrocycles does not bear the cost of “de-mixing” the polar solvent such as methanol from the nonpolar hexane/ethyl acetate. Water has a much higher cohesive energy density than methanol (2294 vs 858 MPa),²⁹ meaning that the tendency for the “activated” water molecules inside the macrocycles to aggregate in membranes is much stronger than that for the methanol in mixed organic solvent. The concentration of the oligocholates in the membrane (i.e., up to 5 mol % with respect to the phospholipids) was much higher than that used in the fluorescence quenching experiments (i.e., 2.0 μ M), making aggregation of the oligocholates much easier in the membranes than in the mixed organic solvents.

Both the pyrene–excimer formation and the glucose leakage assay indicate that the all-amide-linked macrocycles were better at stacking than the clicked ones. The results are reasonable considering that the proposed hydrophobic stacking needs the reverse micelle-like configuration of the macrocycles with introverted polar groups. The clicked macrocycles are larger than the amide-linked ones and also have more rotatable bonds—both factors make it easier for the cholate to twist and turn the introverted hydroxyl groups outward. Such motion not only reduces the solvophobic driving force of the stacking but also makes the interior of the nanopore less hydrophilic even if the pore is formed. Glucose leakage is expected to be difficult and was indeed observed with the clicked macrocycles (Figure 8a).

What then is the reason for the enhanced quenching found for the clicked macrocycles in mixed organic solvents (Figure 3a)? A strong possibility is that the quenching of the pyrene-labeled macrocycle 3 by the NDI-labeled 4 in 0.5% methanol was caused not by the solvophobic stacking of the macrocycles but by the cholate units rotating outward and hydrogen-bonding with one another intermolecularly. Such hydrogen-bonded interactions are more likely for the more flexible clicked macrocycles and should be the strongest in the least methanol-containing solvents. Essentially, two different but related mechanisms were operating in solution and in the lipid membrane, respectively. In solution and only in low methanol (0.5%) solutions, the hydrogen-bond-assisted aggregation occurred with the clicked, flexible oligocholate macrocycles (3–5). The polar solvent-induced solvophobic stacking of the macrocycles was probably not strong enough to operate in the mixed organic solvents, due to low concentrations of the macrocycles, good miscibility of methanol/ethyl acetate/hexane, and the low cohesive energy density of methanol.

CONCLUSIONS

This study yielded additional insight into the hydrophobic stacking of the oligocholate macrocycles in lipid membranes. Mechanistically, the aggregation of the amphiphilic macrocycles is similar to the formation or reverse micelles by a head/tail surfactant in nonpolar solvents in the presence of a small amount of water.³⁰ Both the stacking of the macrocycles and the aggregation of surfactants to form reverse micelles are driven by the same solvophobic interactions—i.e., the tendency of the polar groups to avoid contact with the bulk, nonpolar solvent and the strong preference of water molecules to

associate with water instead of the nonpolar solvent. The different self-assembled structures (i.e., water-filled nanopores vs spherical, water-filled reverse micelles) simply result from the different topologies of the amphiphiles.

The effectiveness of the NDI group in lipid membranes is noteworthy. The aromatic donor–acceptor interactions between an NDI and a 1,5-dialkoxynaphthalene derivative were found to be 1–2 orders of magnitude stronger than the acceptor–acceptor interactions in several *polar* solvents.³¹ Our leakage data, however, clearly shows that the acceptor–acceptor interactions were more effective at promoting the stacking of the oligocholate macrocycles. Our current explanation for the result was based on the solvation of the NDI group in *nonpolar* environments. In our experience, compounds with the NDI group tend to have much poorer solubility than pyrene derivatives in common organic solvents including hydrocarbons. The poor solubility probably comes from the strong intermolecular interactions of the NDI groups and its poor solvation by common organic solvents. When the NDI-functionalized oligocholates enter the lipid membrane, the poor solubility of the NDI group in hydrocarbons translates to a stronger tendency to aggregate in lipid hydrocarbon and was clearly beneficial to the transport ability of macrocycle **8**.

EXPERIMENTAL SECTION

The syntheses of compound **3**,^{14a} **6**,^{14a} **9**,³² **10**,²¹ **11**,^{19c} **12**,^{14a} **16**,^{14a} **17**,³² and **18**³² were previously reported. The preparation of LUVs,³² the procedures for the leakage assays,³² and the incorporation of oligocholates into liposomes by detergent dialysis and direct addition to preformed LUVs^{14a} were reported previously.

General Methods. For spectroscopic purposes, methanol, hexanes, and ethyl acetate were of HPLC grade. All other reagents and solvents were of ACS-certified grade or higher and were used as received from commercial suppliers.

Compound 4. The amine derivative^{14a} of compound **6** (50 mg, 0.037 mmol), compound **17** (56 mg, 0.108 mmol), and diisopropylethylamine (DIPEA, 32 μ L, 0.184 mmol) were dissolved in anhydrous DMF (0.2 mL). The mixture was stirred at 50 °C overnight and poured into dilute HCl aqueous solution (0.05 M, 50 mL). The precipitate was collected by suction filtration and purified by preparative TLC using 9:1 CHCl₃/CH₃OH as the developing solvent to afford a light brown powder (36 mg, 50%). ¹H NMR (400 MHz, CDCl₃/CD₃OD = 1:1, δ): 8.68 (s, 4H), 7.75 (m, 1H), 7.43 (m, 1H), 4.30 (m, 3H), 4.14 (br, 5H), 3.86 (br, 3H), 3.72 (br, 2H), 3.39 (m, 2H), 3.08 (br, 2H), 2.70 (q, 1H), 2.38–1.0 (a series of m), 0.61 (s, 1H). ¹³C NMR (100 MHz, CDCl₃/CD₃OD = 1:1, δ): 175.3, 174.9, 174.5, 171.9, 164.5, 144.5, 131.0, 127.3, 125.9, 125.1, 125.0, 124.9, 124.8, 124.7, 123.3, 120.7, 72.9, 68.0, 61.5, 53.5, 49.6, 46.4, 45.7, 42.2, 39.5, 36.7, 35.7, 34.6, 32.7, 31.8, 29.6, 27.5, 27.1, 26.6, 25.9, 23.1, 22.3, 17.0, 12.2. ESI-HRMS (*m/z*): [M + Na]⁺ calcd for C₁₀₂H₁₄₈N₁₀NaO₁₅ 1776.1018, found 1776.1008.

Compound 5. The amine derivative^{14a} of compound **6** (92 mg, 0.067 mmol), compound **16** (58 mg, 0.169 mmol), and DIPEA (59 μ L, 0.337 mmol) were dissolved in anhydrous DMF (0.3 mL). The mixture was allowed to react in a microwave reactor at 100 °C for 30 min and poured into dilute HCl aqueous solution (0.05 M, 50 mL). The precipitate was collected by suction filtration and purified by preparative TLC using 9:1 CHCl₃/CH₃OH as the developing solvent to afford an off-white powder (50 mg, 45%). ¹H NMR (400 MHz, CDCl₃/CD₃OD = 1:1, δ): 8.60 (br, 1H), 8.42 (br, 1H), 8.26–7.99 (9H), 4.48 (br, 3H), 4.35 (br, 1H), 3.92 (br, 3H), 3.76 (br, 3H), 3.58 (br, 3H), 3.51 (br, 1H), 2.85 (br, 1H), 2.38–1.0 (a series of m), 0.88 (s, 9H), 0.67 (d, 9H). ¹³C NMR (100 MHz, CDCl₃/CD₃OD = 1:1, δ): 175.2, 174.8, 173.7, 171.7, 162.8, 144.7, 130.5, 126.8, 120.8, 73.1, 67.9, 61.6, 56.7, 53.3, 46.5, 39.7, 34.7, 31.9, 29.4, 26.5, 23.3, 20.4, 16.7, 13.4, 11.9. ESI-HRMS (*m/z*): [M + H]⁺ calcd for C₉₇H₁₃₉N₈O₁₁ 1592.0558, found 1592.0570.

Compound 13. Compound **12** (230 mg, 0.156 mmol) and triphenylphosphine (73.7 mg, 0.281 mmol) were dissolved in MeOH (2 mL). The reaction mixture was heated to reflux for overnight. The solvent was removed by rotary evaporation. The residue was purified by column chromatography over silica gel with 15:1 CH₂Cl₂/CH₃OH and then with 6:1:0.1 CH₂Cl₂/CH₃OH/Et₃N (6/1/0.1) as the eluents to afford an off-white powder (103 mg, 46%). ¹H NMR (400 MHz, CD₃OD/CDCl₃ = 1:1, δ): 7.28 (br, 5H), 5.04 (br, 2H), 4.25 (br, 1H), 3.93 (br, 3H), 3.78 (br, 3H), 3.62 (s, 3H), 3.49 (br, 2H), 3.13 (m, 2H), 2.38–1.0 (a series of m), 0.88 (s, 9H), 0.64 (d, 9H). ¹³C NMR (100 MHz, CDCl₃/CD₃OD = 1:1, δ): 175.6, 175.2, 174.5, 171.8, 157.6, 136.9, 128.5, 128.0, 127.8, 73.0, 68.1, 66.6, 61.6, 53.2, 50.7, 48.8, 46.5, 42.8, 41.8, 39.5, 36.3, 35.4, 35.0, 33.6, 32.8, 31.8, 31.1, 29.9, 28.4, 27.7, 26.6, 23.3, 22.5, 18.2, 17.0, 12.6. ESI-HRMS (*m/z*): [M + H]⁺ calcd for C₈₆H₁₃₈N₅O₁₃ 1449.0286, found 1449.0273.

Compound 14. Hydrolyzed compound **13** (50 mg, 0.034 mmol), BOP (75 mg, 0.169 mmol), and HOBT (23 mg, 0.169 mmol) were dissolved in DMF (30 mL), and DIPEA (60 μ L, 0.34 mmol) was added. The mixture was allowed to react in a microwave reactor at 100 °C for 1 h and poured into dilute HCl aqueous solution (0.05 M, 50 mL). The precipitate formed was collected by suction filtration, washed with water, dried in air, and purified by column chromatography over silica gel with 10:1 CH₂Cl₂/CH₃OH as the eluent to afford an ivory powder (47 mg, 98%). ¹H NMR (300 MHz, CD₃OD, δ): 7.30 (br, 5H), 5.04 (br, 2H), 4.14 (br, 1H), 3.92 (br, 3H), 3.78 (br, 3H), 3.48 (br, 2H), 3.13 (m, 3H), 2.38–1.0 (a series of m), 0.88 (s, 9H), 0.67 (d, 9H). ¹³C NMR (100 MHz, CDCl₃/CD₃OD = 1:1, δ): 176.7, 175.2, 174.9, 172.3, 158.2, 136.9, 128.5, 128.0, 127.8, 73.0, 68.1, 66.6, 61.6, 53.2, 50.7, 48.8, 46.5, 42.8, 41.8, 39.5, 36.3, 35.4, 35.0, 33.6, 32.8, 31.8, 31.1, 29.9, 28.4, 27.7, 26.6, 23.3, 22.2, 19.1, 16.8, 12.8. ESI-HRMS (*m/z*): [M + Na]⁺ calcd for C₈₅H₁₃₃N₅O₁₂Na 1438.9843, found 1438.9833.

Compound 15. Pd/C (240 mg, 10 wt %) was added to a solution of **5** (236 mg, 0.167 mmol) in CH₃OH (20 mL). The mixture was stirred under a H₂ balloon at room temperature for 3 d. Pd/C was removed by filtration through a pad of Celite, and the solvent was removed by rotary evaporation to afford a white powder (150 mg, 80%). ¹H NMR (300 MHz, CD₃OD, δ): 4.23 (br, 1H), 3.93 (br, 3H), 3.78 (br, 3H), 3.47 (br, 3H), 2.74–0.98 (a series of m), 0.89 (s, 9H), 0.67 (d, 9H). ¹³C NMR (100 MHz, CDCl₃/CD₃OD = 1:1, δ): 176.8, 175.4, 175.1, 172.6, 158.5, 136.9, 73.0, 68.1, 66.6, 53.2, 50.7, 48.8, 46.5, 42.8, 41.8, 39.5, 36.3, 35.4, 35.0, 33.6, 32.8, 31.8, 31.1, 29.9, 28.4, 27.7, 26.6, 23.3, 22.2, 19.3, 16.6, 12.4. ESI-HRMS (*m/z*): [M + H]⁺ calcd for C₇₇H₁₂₈N₅O₁₀ 1282.9656, found 1282.9645.

Compound 7. Compound **15** (80 mg, 0.062 mmol), compound **16** (72 mg, 0.187 mmol), and DIPEA (109 μ L, 0.624 mmol) were dissolved in anhydrous DMF (0.2 mL). The mixture was stirred at 60 °C overnight and poured into a dilute HCl aqueous solution (0.05 M, 30 mL). The precipitate was collected by suction filtration and purified by preparative TLC using 9:1 CHCl₃/CH₃OH as the developing solvent to afford an off-white powder (40 mg, 42%). ¹H NMR (400 MHz, CDCl₃/CD₃OD = 1:1, δ): 8.30 (m, 2H), 8.09 (m, 4H), 7.98 (m, 2H), 7.84 (m, 1H), 4.21 (m, 1H), 3.90 (br, 3H), 3.77 (br, 3H), 3.59 (q, 2H), 3.50 (br, 3H), 2.92 (m, 2H), 2.46 (br, 2H), 2.38–1.0 (a series of m), 0.58 (m, 7 H), 0.44 (s, 2H). ¹³C NMR (100 MHz, CDCl₃/CD₃OD = 1:1, δ): 175.3, 174.9, 174.5, 171.9, 144.5, 136.0, 127.3, 125.9, 125.1, 125.0, 124.9, 124.8, 124.7, 123.3, 120.7, 72.9, 68.0, 61.5, 53.5, 49.6, 46.4, 45.7, 42.2, 39.5, 36.7, 35.7, 34.6, 32.7, 31.8, 29.6, 27.5, 27.1, 26.6, 25.9, 23.1, 22.3, 17.0, 12.2. ESI-HRMS (*m/z*): [M + H]⁺ calcd for C₉₇H₁₄₂N₅O₁₁ 1553.0700, found 1553.0687.

Compound 8. Compound **15** (55 mg, 0.043 mmol), compound **17** (65 mg, 0.129 mmol), and DIPEA (37 μ L, 0.215 mmol) were dissolved in anhydrous DMF (0.2 mL). The mixture was stirred at 60 °C overnight and poured into a dilute HCl aqueous solution (0.05 M, 30 mL). The precipitate was collected by suction filtration and purified by preparative TLC using 9:1 CHCl₃/CH₃OH as the developing solvent to afford an off-white powder (52 mg, 72%). ¹H NMR (400 MHz, CDCl₃/CD₃OD = 1:1, δ): 8.73 (s, 4H), 4.24 (m, 4H), 3.94 (br, 3H), 3.79 (br, 3H), 3.52 (q, 2H), 3.17 (br, 3H), 2.45–0.73 (a series of m), 0.66 (m, 9 H). ¹³C NMR (100 MHz, CDCl₃/CD₃OD = 1:1, δ):

177.6, 176.2, 175.2, 163.7, 131.6, 127.3, 73.6, 68.5, 62.6, 52.8, 47.9, 46.7, 42.7, 39.9, 36.9, 36.0, 35.2, 32.4, 31.6, 28.6, 28.4, 27.3, 23.2, 17.7, 14.3, 12.9. ESI-HRMS (m/z): $[M + H_3O]^+$ calcd for $C_{99}H_{148}N_7O_{16}$ 1692.1016 found, 1692.0574.

Fluorescence Titrations. Stock solutions (5×10^{-4} M) of the appropriate oligocholate pyrene–NDI pairs in anhydrous THF were prepared. An aliquot (8.0 μ L) of the stock solution was added to 2.00 mL of hexane/ethyl acetate ($v/v = 2/1$) containing varying amounts of methanol (0.5–15%) in a quartz cuvette. The sample was gently vortexed for 30 s after each addition before the fluorescence spectrum was recorded. The excitation wavelength was 350 nm.

■ ASSOCIATED CONTENT

● Supporting Information

NMR data for the key compounds. This material is available free of charge via the Internet at <http://pubs.acs.org>.

■ AUTHOR INFORMATION

Corresponding Author

*Phone: 515-294-5845. Fax: 515-294-0105. E-mail: zhaoy@iastate.edu.

Notes

The authors declare no competing financial interest.

■ ACKNOWLEDGMENTS

We acknowledge the NSF (DMR-1005515) for support of this research.

■ REFERENCES

- (1) (a) Stein, W. D. *Carriers and Pumps: An Introduction to Membrane Transport*; Academic Press: San Diego, 1990. (b) Gokel, G. W.; Carasel, I. A. *Chem. Soc. Rev.* **2007**, *36*, 378–389. (c) Fyles, T. M. *Chem. Soc. Rev.* **2007**, *36*, 335–347. (d) McNally, B. A.; Leevy, W. M.; Smith, B. D. *Supramol. Chem.* **2007**, *19*, 29–37. (e) Davis, J. T.; Okunola, O.; Quesada, R. *Chem. Soc. Rev.* **2010**, *39*, 3843–3862.
- (2) Litvinchuk, S.; Sorde, N.; Matile, S. *J. Am. Chem. Soc.* **2005**, *127*, 9316–9317.
- (3) Sakai, N.; Sorde, N.; Matile, S. *J. Am. Chem. Soc.* **2003**, *125*, 7776–7777.
- (4) (a) Matile, S.; Som, A.; Sorde, N. *Tetrahedron* **2004**, *60*, 6405–6435. (b) Sisson, A. L.; Shah, M. R.; Bhosale, S.; Matile, S. *Chem. Soc. Rev.* **2006**, *35*, 1269–1286.
- (5) (a) Gokel, G. W.; Mukhopadhyay, A. *Chem. Soc. Rev.* **2001**, *30*, 274–286. (b) Koert, U.; Al-Momani, L.; Pfeifer, J. R. *Synthesis* **2004**, 1129–1146. (c) Gokel, G. W.; Murillo, O. *Acc. Chem. Res.* **1996**, *29*, 425–432. (d) Jung, M.; Kim, H.; Baek, K.; Kim, K. *Angew. Chem., Int. Ed.* **2008**, *47*, 5755–5757. (e) Li, X.; Shen, B.; Yao, X. Q.; Yang, D. *J. Am. Chem. Soc.* **2009**, *131*, 13676–13680.
- (6) Som, A.; Matile, S. *Chem. Biodiv.* **2005**, *2*, 717–729.
- (7) (a) Granja, J. R.; Ghadiri, M. R. *J. Am. Chem. Soc.* **1994**, *116*, 10785–10786. (b) Sanchez-Quesada, J.; Kim, H. S.; Ghadiri, M. R. *Angew. Chem., Int. Ed.* **2001**, *40*, 2503–2506.
- (8) (a) Sakai, N.; Mareda, J.; Matile, S. *Acc. Chem. Res.* **2005**, *38*, 79–87. (b) Das, G.; Talukdar, P.; Matile, S. *Science* **2002**, *298*, 1600–1602.
- (9) Bhosale, S.; Sisson, A. L.; Talukdar, P.; Furstenberg, A.; Banerji, N.; Vauthey, E.; Bollot, G.; Mareda, J.; Roger, C.; Wurthner, F.; Sakai, N.; Matile, S. *Science* **2006**, *313*, 84–86.
- (10) Satake, A.; Yamamura, M.; Oda, M.; Kobuke, Y. *J. Am. Chem. Soc.* **2008**, *130*, 6314–6315.
- (11) Helsel, A. J.; Brown, A. L.; Yamato, K.; Feng, W.; Yuan, L. H.; Clements, A. J.; Harding, S. V.; Szabo, G.; Shao, Z. F.; Gong, B. *J. Am. Chem. Soc.* **2008**, *130*, 15784–15785.
- (12) Fyles, T. M.; Tong, C. C. *New J. Chem.* **2007**, *31*, 655–661.
- (13) Ma, L.; Melegari, M.; Colombini, M.; Davis, J. T. *J. Am. Chem. Soc.* **2008**, *130*, 2938–2939.

(14) (a) Cho, H.; Widanapathirana, L.; Zhao, Y. *J. Am. Chem. Soc.* **2011**, *133*, 141–147. (b) Cho, H.; Zhao, Y. *Langmuir* **2011**, *27*, 4936–4944.

(15) Dunitz, J. D. *Science* **1994**, *264*, 670.

(16) (a) Hunter, C. A.; Lawson, K. R.; Perkins, J.; Urch, C. J. *J. Chem. Soc., Perkin Trans. 2* **2001**, 651–669. (b) Waters, M. L. *Curr. Opin. Chem. Biol.* **2002**, *6*, 736–741.

(17) (a) Philp, D.; Stoddart, J. F. *Angew. Chem., Int. Ed. Engl.* **1996**, *35*, 1154–1196. (b) Scott Lokey, R.; Iverson, B. L. *Nature* **1995**, *375*, 303–305. (c) Gabriel, G. J.; Sorey, S.; Iverson, B. L. *J. Am. Chem. Soc.* **2005**, *127*, 2637–2640. (d) Nelson, J. C.; Saven, J. G.; Moore, J. S.; Wolynes, P. G. *Science* **1997**, *277*, 1793–1796. (e) Stone, M. T.; Heemstra, J. M.; Moore, J. S. *Acc. Chem. Res.* **2006**, *39*, 11–20. (f) Huc, I. *Eur. J. Org. Chem.* **2004**, 17–29.

(18) For other related cyclic cholate derivatives, see: (a) Brady, P. A.; Bonar-Law, R. P.; Rowan, S. J.; Suckling, C. J.; Sanders, J. K. M. *Chem. Commun.* **1996**, 319–320. (b) Davis, A. P.; Walsh, J. J. *Chem. Commun.* **1996**, 449–451. (c) Whitmarsh, S. D.; Redmond, A. P.; Sgarlata, V.; Davis, A. P. *Chem. Commun.* **2008**, 3669–3671. (d) Ghosh, S.; Choudhury, A. R.; Row, T. N. G.; Maitra, U. *Org. Lett.* **2005**, *7*, 1441–1444. (e) Albert, D.; Feigel, M.; Benet-Buchholz, J.; Boese, R. *Angew. Chem., Int. Ed.* **1998**, *37*, 2727–2729. (f) Feigel, M.; Ladberg, R.; Winter, M.; Blaser, D.; Boese, R. *Eur. J. Org. Chem.* **2006**, 371–377.

(19) (a) Zhao, Y.; Zhong, Z.; Ryu, E.-H. *J. Am. Chem. Soc.* **2007**, *129*, 218–225. (b) Cho, H.; Zhong, Z.; Zhao, Y. *Tetrahedron* **2009**, *65*, 7311–7316. (c) Cho, H.; Zhao, Y. *J. Am. Chem. Soc.* **2010**, *132*, 9890–9899. (d) Zhong, Z.; Li, X.; Zhao, Y. *J. Am. Chem. Soc.* **2011**, *133*, 8862–8865.

(20) Rostovtsev, V. V.; Green, L. G.; Fokin, V. V.; Sharpless, K. B. *Angew. Chem., Int. Ed.* **2002**, *41*, 2596–2599.

(21) Zhao, Y.; Zhong, Z. *J. Am. Chem. Soc.* **2005**, *127*, 17894–17901.

(22) Normalization allows us to compare the different pyrene-labeled oligocholates more accurately. These compounds have different structures and thus potentially different solvent shells around the fluorophore in the mixed polar/nonpolar solvents. Because fluorescence is often sensitive to the solvent composition around the fluorophore, the different pyrene-labeled oligocholates may not be comparable directly.

(23) Lande, M. B.; Donovan, J. M.; Zeidel, M. L. *J. Gen. Physiol.* **1995**, *106*, 67–84.

(24) Birks, J. B.; Munro, I. H.; Dyson, D. J. *Proc. R. Soc. London Ser. A* **1963**, *275*, 575–588.

(25) Kinsky, S. C.; Haxby, J. A.; Zopf, D. A.; Alving, C. R.; Kinsky, C. B. *Biochemistry* **1969**, *8*, 4149–&.

(26) Nezil, F. A.; Bloom, M. *Biophys. J.* **1992**, *61*, 1176–1183.

(27) Holthuis, J. C. M.; van Meer, G.; Huitema, K. *Mol. Membr. Biol.* **2003**, *20*, 231–241.

(28) (a) Demel, R. A.; Bruckdor, Kr; Vandeene, L. *Biochim. Biophys. Acta* **1972**, *255*, 321–330. (b) Papahadjopoulos, D.; Nir, S.; Ohki, S. *Biochim. Biophys. Acta* **1972**, *266*, 561–583.

(29) Reichardt, C. In *Solvents and Solvent Effects in Organic Chemistry*, 3rd ed.; Wiley-VCH: Weinheim, 2003; p 63.

(30) Pileni, M. P. *Structure and Reactivity in Reverse Micelles*; Elsevier: Amsterdam, 1989.

(31) Cubberley, M. S.; Iverson, B. L. *J. Am. Chem. Soc.* **2001**, *123*, 7560–7563.

(32) Zhang, S.; Zhao, Y. *Chem.—Eur. J.* **2011**, *17*, 12444–12451.